Investigation of the characteristics of a stacked direct borohydride fuel cell for portable applications

Cheolhwan Kim [a], Kyu-Jung Kim [a], Man Yeong Ha [b],*

[a] *Digital Appliance Company Laboratory, LG Elecrtronics, 391-2, Gaeumjeong-Dong, Changwon City, Gyeongnam 641-711, Republic of Korea*
[b] *School of Mechanical Engineering, Pusan National University, San 30, Jangjeon-Dong, Kumjeong-Ku, Pusan 609-735, Republic of Korea*

Abstract

To investigate the possibility of the portable application of a direct borohydride fuel cell (DBFC), weight reduction of the stack and high stacking of the cells are investigated for practical running conditions. For weight reduction, carbon graphite is adopted as the bipolar plate material even though it has disadvantages in tight stacking, which results in stacking loss from insufficient material strength. For high stacking, it is essential to have a uniform fuel distribution among cells and channels to maintain equal electric load on each cell. In particular, the design of the anode channel is important because active hydrogen generation causes non-uniformity in the fuel flow-field of the cells and channels. To reduce the disadvantages of stacking force margin and fuel maldistribution, an O-ring type-sealing system with an internal manifold and a parallel anode channel design is adopted, and the characteristics of a single and a five-cell fuel cell stack are analyzed. By adopting carbon graphite, the stack weight can be reduced by 4.2 times with 12% of performance degradation from the insufficient stacking force. When cells are stacked, the performance exceeds the single-cell performance because of the stack temperature increase from the reduction of the radiation area from the narrow stacking of cells.
© 2008 Elsevier B.V. All rights reserved.

Keywords: Direct borohydride fuel cell; Hydrogen generation; Carbon graphite; Maldistribution; Stacked cell; Two-phase flow

1. Introduction

Fuel cells are not only of interest for large-scale applications, but are also being considered as a power source for portable usages. For portable applications, liquid fuel is considered to be the solution in view of volumetric energy density [1–5]. Recently, a sodium borohydride aqueous solution has become an interesting alternative as a liquid fuel for fuel cells due to its many advantageous features such as high-energy capacity and safety [6–13]. Moreover, non-precious materials can be used to catalyze the anodic reaction.

Direct borohydride fuel cell (DBFC) uses a sodium borohydride (NaBH$_4$) solution as fuel, and electricity is produced via the following reaction:

$$NaBH_4 + 2O_2 \rightarrow NaBO_2 + 2H_2O \qquad E^\circ = 1.64\,V \qquad (1)$$

Amendola et al. [4] suggested a simple process to generate hydrogen gas from aqueous solutions of NaBH$_4$ by using a ruthenium catalyst. Rapid hydrogen generation rates were achieved using a NaBH$_4$ solution with 5 wt.% ruthenium. Suda [5] suggested a simple and efficient method for the generation of hydrogen gas, in which a reaction medium is prepared by dissolution of a metal hydrogen complex compound. As a catalyst, they used metals such as cobalt, nickel or hydrogen-absorbing alloys so that the decomposition of the metal hydrogen complex compound proceeds, even at room temperature, to generate hydrogen gas. It was found that the catalytic activity of the catalyst could be increased by subjecting the catalyst to a fluorinating treatment. However, hydrogen generation not only decreases fuel utilization, but also lowers cell performance, because hydrogen bubbles hinder ion movement in the anolyte. This hydrogen can be generated not only from the hydrolysis reaction but also from the electrochemical reaction [6,7].

Kojima et al. [14] found that Pt–LiCoO$_2$ worked as an excellent catalyst to release hydrogen from the stabilized NaBH$_4$ solution because small metal crystallites increase the hydrogen generation rate. Kojima et al. [15] measured hydrogen yield to

* Corresponding author. Tel.: +82 51 510 2440; fax: +82 51 512 9835.
  E-mail address: myha@pusan.ac.kr (M.Y. Ha).

Nomenclature

$H_{air,in}$	inlet air humidity (%)
I	electric current (A)
P_{air}	air side pressure (kPa)
P_{fuel}	fuel side pressure (kPa)
ΔP_{air}	air side pressure loss (Pa)
ΔP_{fuel}	fuel side pressure loss (Pa)
Q_{air}	air volume flow rate (l min^{-1})
Q_{fuel}	fuel volume flow rate (l min^{-1})
Q_h	hydrogen flow rate (l min^{-1})
$T_{air,in}$	inlet air temperature (°C)
$T_{air,out}$	outlet air temperature (°C)
$T_{air,out,exp}$	measured outlet air temperature (°C)
$T_{air,out,reg}$	regressed outlet air temperature (°C)
$T_{fuel,in}$	inlet fuel temperature (°C)
$T_{fuel,out}$	outlet fuel temperature (°C)
$T_{fuel,out,exp}$	measured outlet fuel temperature (°C)
$T_{fuel,out,reg}$	regressed outlet fuel temperature (°C)
T_{wall}	stack wall temperature (°C)
$T_{wall,exp}$	measured stack wall temperature (°C)
$T_{wall,reg}$	regressed stack wall temperature (°C)
W_{stack}	stack power (W)

use a fuel for uninterrupted power supply. They found that the yield by the hydrolysis reaction of LiBH$_4$ was accelerated when a small amount of water was used. Liu et al. [16] developed catalysts based on nickel and cobalt to accelerate the hydrolysis reaction for hydrogen generation. They showed that cobalt had higher catalytic activity than nickel in most cases, but Raney nickel demonstrated the best performance. Ha et al. [17] sug-

gested a practical design to solve maldistribution in liquid fuel cells through simulation and experiment. Li et al. [18] achieved 290 mW cm^{-2} from a direct borohydride fuel cell using a palladium mixture in the anode, and demonstrated 110 W with a five-cell stack with an effective area of 67 cm^2 when the operation temperature reached 60 °C. Kim et al. [19,20] assembled a single cell, of which the active area was 100 cm^2, with a corrugated shaped anode, and achieved 218 mW cm^{-2}.

In this study, the possibility of weight reduction of a DBFC is investigated, and the characteristics of a five-cell DBFC are analyzed under practical running conditions for portable applications.

2. Experimental methodology

2.1. Experimental apparatus

Fig. 1 shows a schematic of the experimental apparatus employed to measure the performance of a DBFC. The experimental apparatus consists of different parts: a water bath, fuel and air supply, electric load and hood.

The capacity of the stainless-steel water bath, which was fitted with a heater and motor for circulation, was 20 l. A fuel tank was stored in the bath for temperature control and was properly maintained at a constant temperature by heat transfer with the water flow in the bath.

Fuel was supplied to the stack using a metering pump from a fuel tank with a diameter of 200 mm and a height of 300 mm. The fuel was supplied through a 6 mm diameter Teflon tube to the stack. At the inlet and outlet of the stack, pressure gauges and thermometers were installed to measure the fuel condition. When the reaction was finished in the stack, the fuel was returned to the top of the fuel tank and separated into gas and liquid. The
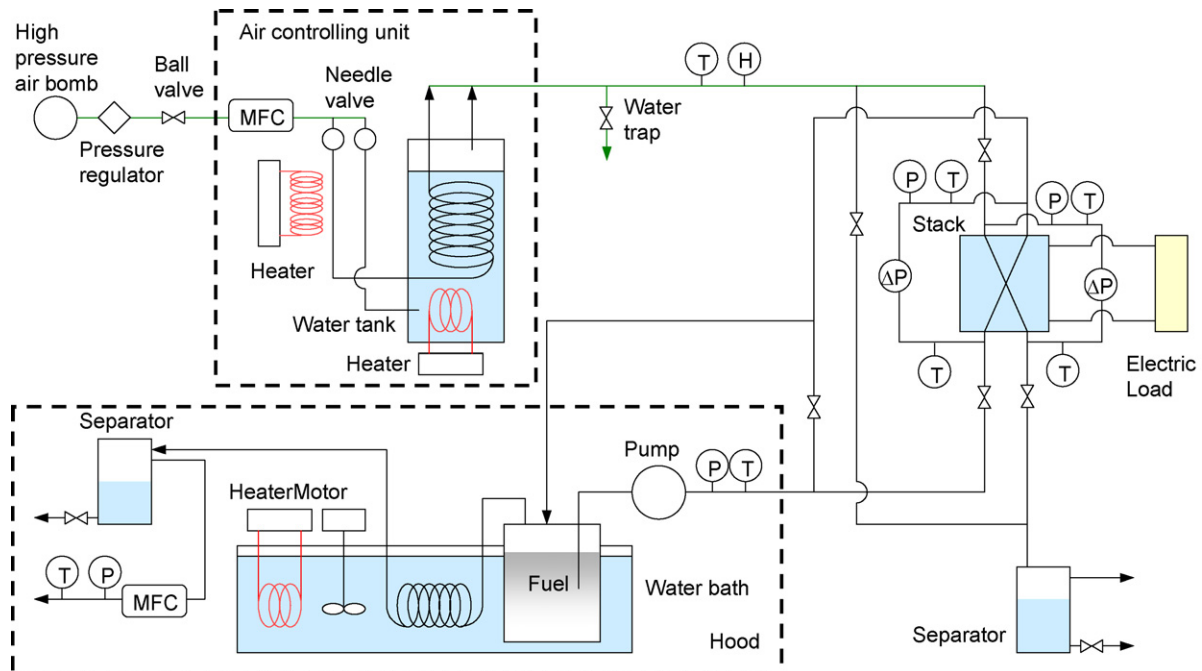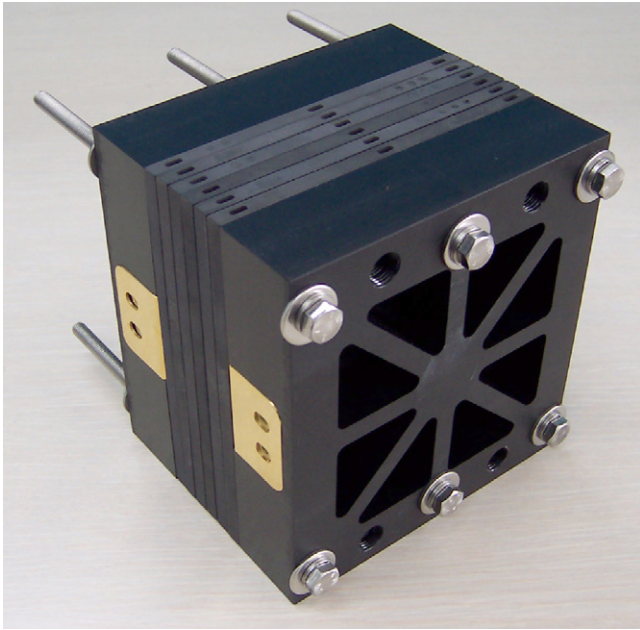

Fig. 1. Schematic of experimental apparatus.

Fig. 2. Photograph of five-cell fuel cell stack.

liquid fuel was cooled in the water bath and re-circulated to the stack. The gaseous fuel was also cooled while passing through a submerged spiral tube whose diameter and length were 6.4 mm and 1.5 m, respectively. The volume of the fuel gas was measured by a hydrogen flow meter, and then finally released into the atmosphere through the hood.

Dry air was supplied from a high-pressure air bomb and its pressure was reduced by a pressure regulator. The flow rate of air was controlled by an air flow meter. The dry air was humidified and heated while it passed through a bubbler and a spiral heating tube. The humidity and temperature of the air was controlled by changing the distribution rate of the air flow to the bubbler and the heating tube. After passing through the air control unit, the wet air reached the stack and reacted in the cathode, and then was fed to the separator for evacuation.

A 100 W grade electric load with a fixed current mode was used to measure the performance of the stack.

2.2. Test section

Fig. 2 shows the test section. This includes a five-cell DBFC and measuring devices. Thermometers and pressure transducers were installed at the inlet and the outlet of the air and fuel channels, and differential pressure transducers were connected to measure the pressure drop between the inlets and the outlets. An electric circuit was connected to each cell to measure the respective voltages. The stack consists of two end-plates, four bipolar plates and five membrane electrode assemblies (MEAs). The end-plates and the bipolar plates were made from carbon graphite.

Fig. 3 shows the anode-side and cathode-side end-plates. Parallel channels were used to match with the corrugated-shaped anode. The spacing, wall thickness and height of the channel are 2.7, 0.5 and 2.0 mm, respectively. Each wall is 15-mm long with a 5 mm space in the lengthwise direction for effective exhaust of hydrogen gas. For a smooth discharge of sodium hydroxide generated from the reaction, a serpentine channel was adopted for the cathode channel. A set of five channels having a hydraulic diameter of 1.2 mm was used.

A corrugated anode [19], a gold-coated stainless-steel mesh, a cation-exchange membrane and a Pt 5 wt.%–C on carbon cloth substrate were used to give a MEAs with a 72 cm^2 effective area. The aspect ratio is 1.0, and the length of one side is 85 mm. For the anode fuel, a borohydride solution containing 10 wt.% $NaBH_4$ was prepared by dissolving sodium borohydride in a 20 wt.% NaOH solution. Humidified air is supplied for the cathodic oxidant. A heat pipe module was set at the top of the stack for its cooling. Four T-type thermocouples were placed at the top, sides and bottom of the stack wall [20].

2.3. Test method

A pressure regulator in the air side was turned on when the bubbler temperature reached the target temperature, and the flow rate was controlled by a flow controller. At the same time, a valve in the water trap was opened to evacuate the humid air

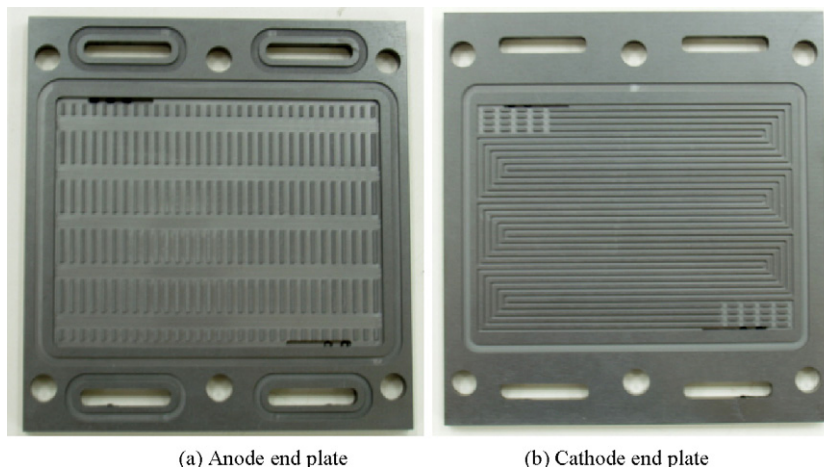(a) Anode end plate   (b) Cathode end plate

Fig. 3. Photographs of end-plates.

into the atmosphere until the targetted experimental condition was satisfied.

One kilogram of fuel was prepared in the fuel tank which was submerged in the water bath to adjust the fuel temperature. If the fuel temperature was within the targetted value, the fuel pump was turned on to circulate fuel in the stack. The experiment started when the air and fuel condition was satisfied by closing the valve in the air-side water trap. The air flow rate was varied from 10 to $40 \, l \, min^{-1}$ and the fuel flow-rate from 25×10^{-3} to $100 \times 10^{-3} \, l \, min^{-1}$.

The electric load was set to a constant-current mode, and it was increased or decreased stepwise. When the stack wall temperature exceeded $70 \, °C$, the heat pipe-cooling module was turned on for the safety of the membrane.

3. Results and discussion

3.1. Performance of single and five-cell fuel cell stack

Performance enhancement is one of the most important issues for the application of DBFC as a product. Many researchers have studied the performance enhancement of DBFC, and they have reported positive results [5,18–20], but these studies tend to be confined to the enhancement of the performance of a single cell. To produce a practical fuel cell system, it is advantageous to build cells with as many stacks as possible to obtain a higher electric voltage. This will help achieve higher efficiency in the power converter. On the other hand, the higher stacking of cells increases the possibility of maldistribution in the anode fuel and cathode oxidant. This is one of the main contributions to stacking loss [21]. To reduce this loss, an even distribution of the fuel needs to be considered when designing the manifold. Especially, DBFC uses a liquid fuel in the anode, and two-phase flow occurs in the channel because of the hydrogen generation [3,4,6,7,10,20], so a severe pressure drop and pressure fluctuation in the anode channel is expected. This will induce unstable system operation and a local failure of the fuel supply [21].

Another important issue is weight minimization of the system components. The stack is one of the heaviest components in DBFC, because it is easy to secure safety and to obtain stable results by using metallic materials for the bipolar plates. To reduce the stack weight, the metallic material can be substituted with carbon graphite as in the proton-exchange membrane (PEM) fuel cell. As shown in Table 1, carbon graphite is 4.2 times lighter and has a 3.8 times higher thermal conductivity than that of stainless steel, so the stack weight can be easily reduced and a simpler cooling design can be used by adopting carbon graphite as the bipolar plate, even though it has disadvan-

tages in terms of electrical resistance and tight stacking. When cells are assembled, bipolar plates and MEAs should be tight to provide a smooth migration of ions and electrons. If the contact is not good, the ohmic loss will increase from an insufficient active area and there by cause a degradation of the stack performance. To secure tight contact, a high force is usually applied in the stack assemble process, but carbon graphite is not strong enough to withstand such a force. The adjustment of the stacking force is serious given to the increase in the cell size and numbers [22], so a new sealing system is needed for DBFC to achieve better contact with less stacking force to adopt a light material for the bipolar plate.

To investigate the possibility of using a light material and high stacking in DBFC, a carbon graphite and a stainless-steel bipolar plate were designed in which a parallel-type anode channel with internal-manifolds were considered in one body, while a serpentine channel was applied in the cathode channel. An O-ring type sealing system was applied to secure tight contact between the bipolar plate and the MEA with a smaller stacking force. For the carbon graphite cell, the stacking force was reduced to 30% of that of the stainless-steel cell, because bending of the plate was observed to arise from that stacking force. A five-cell fuel cell stack was assembled using carbon graphite and stainless steel.

Fig. 4 shows the characteristics of power density and cell voltage as a function of current density. The maximum performance of the stainless-steel single cell was $200 \, mW \, cm^{-2}$ which was higher than that of the carbon graphite version by 12%. This was due to the reduced stacking force. Three times more stacking force was applied to the stainless-steel cell, and therefore the contact between the end-plate and the MEA would be tighter than that of the carbon graphite. The effect of the electrical resistance of the materials can be ignored because the minimum plate thickness is 1 mm, so the contribution to the voltage drop is insignificant compared with the voltage difference between the stainless steel and the carbon graphite cells.

The maximum performance of the five-cell carbon graphite fuel cell was $183.8 \, mW \, cm^{-2}$ which is 4% higher than that of the
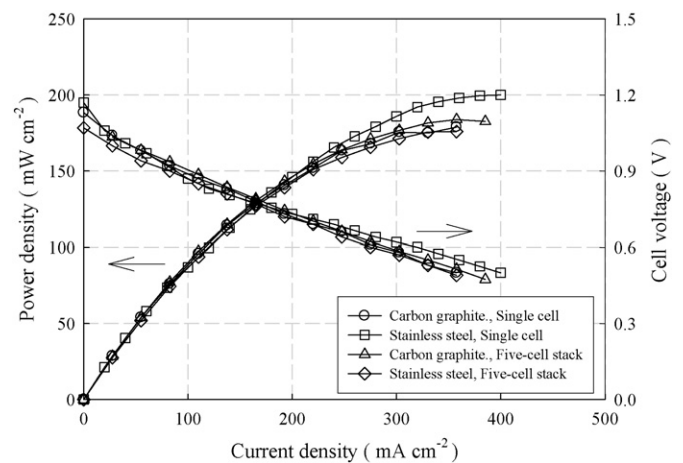
Table 1
Comparison of physical properties of stainless steel and carbon graphite

Property	Stainless steel	Carbon graphite
Electrical resistance ($\Omega \, cm$)	7.2×10^{-5}	80×10^{-5}
Modulus of elasticity (GPa)	200	24
Specific gravity ($g \, cm^{-3}$)	8.02	1.92
Thermal conductivity ($W \, m^{-1} \, K^{-1}$)	16.2	50

Fig. 4. Stack performance as function of current density according to stacking number and plate material. Air flow rate: $10 \, l \, min^{-1}$ ($20 \, l \, min^{-1}$ for five-cell fuel cell stack). Air inlet temperature: $60 \, °C$. Air humidity: 100%. Fuel flow rate: $53 \times 10^{-3} \, l \, min^{-1}$. Fuel inlet temperature: $35 \, °C$.
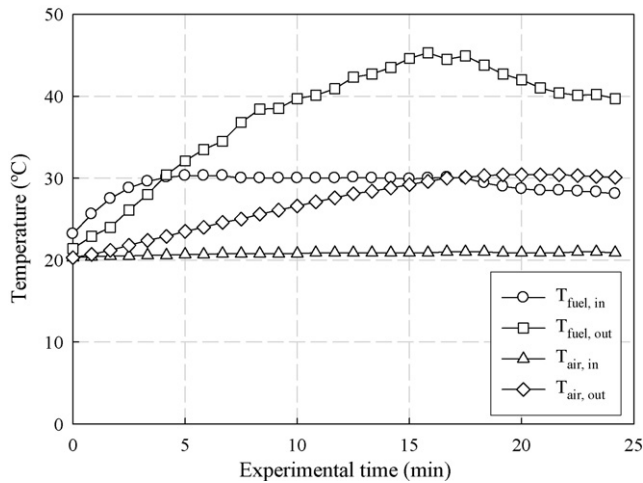
Fig. 5. Inlet and outlet temperatures of fuel and air as function of experimental time. $Q_{air} = 20\,l\,min^{-1}$, $T_{air,in} = 21\,°C$, $H_{air,in} = 100\%$, $Q_{fuel} = 53 \times 10^{-3}\,l\,min^{-1}$, $T_{fuel,in} = 30\,°C$, and $I = 5\,A$.

five-cell stainless-steel fuel cell. It is normal to obtain a lower performance when cells are stacked in a fuel cell system [21], but the results show unusually high stack performance. To explain the phenomena, more detailed analysis on the stacked cell is required.

3.2. Parametric analysis of five-cell fuel cell stack according to experimental time

To understand the characteristics of the stacked cell, a five-cell carbon graphite fuel cell was prepared, and the performance phenomena were analyzed according to the experimental time. Figs. 5–8 present the experimental data of the five-cell carbon graphite fuel cell when the air inlet flow rate, temperature and humidity were fixed at $20\,l\,min^{-1}$, $21\,°C$ and 100%, respectively. The fuel flow rate and temperature were fixed at $53 \times 10^{-3}\,l\,min^{-1}$ and $30\,°C$, respectively. For the convenience of analysis, an electric load was fixed at a constant current of
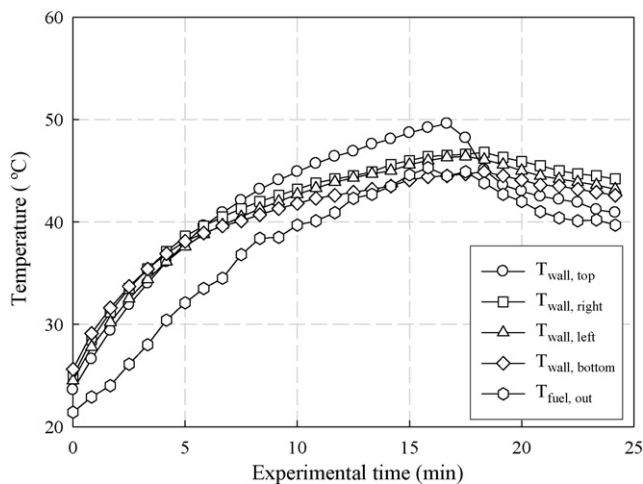

Fig. 6. Temperatures of fuel outlet and stack walls as function of experimental time. $Q_{air} = 20\,l\,min^{-1}$, $T_{air,\,in} = 21\,°C$, $H_{air,in} = 100\%$, $Q_{fuel} = 53 \times 10^{-3}\,l\,min^{-1}$, $T_{fuel,in} = 30\,°C$, and $I = 5\,A$.
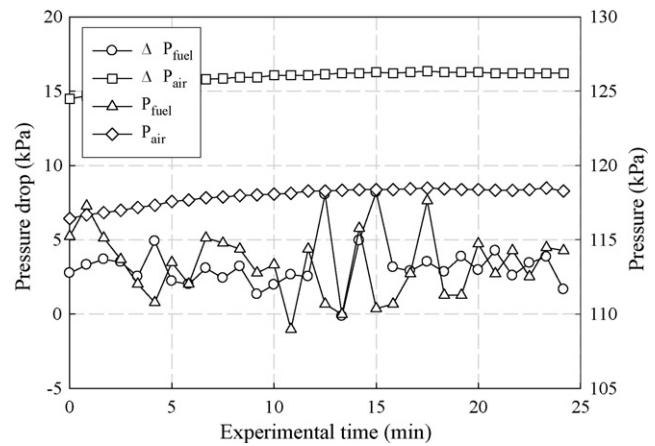

Fig. 7. Pressure and pressure drop of fuel and air as function of experimental time. $Q_{air} = 20\,l\,min^{-1}$, $T_{air,in} = 21\,°C$, $H_{air,in} = 100\%$, $Q_{fuel} = 53 \times 10^{-3}\,l\,min^{-1}$, $T_{fuel,in} = 30\,°C$, and $I = 5\,A$.

5 A. Data were collected for 25 min to analyze the relations of parameters with experimental time. The heat pipe-cooling module was turned on 17 min after starting to check the existence of a hysteresis.

Fig. 5 shows the trend of the inlet and outlet temperatures of the fuel and air. According to the ohmic loss and hydrolysis reaction, thermal energy is generated in the stack proportional to the output power, which causes an increase in the system temperature. When the air inlet temperature is stable at $21\,°C$, the air outlet temperature increases linearly until it reaches $30\,°C$. It peaks at $30\,°C$ after turning on the heat pipe-cooling module. For the fuel, the temperature takes time to stabilize because the system is a closed loop. The fuel inlet temperature linearly increases for the first 5 min, peaks at $30\,°C$, then decreases to $28\,°C$ after the cooling module is turned on. The fuel outlet temperature changes more dramatically. It increases linearly until the cooling started, and then decreases to level off at $40\,°C$. It appears that the effect of the temperature change is more pronounced at the fuel side than that at the air side because the active generation of hydrogen causes fuel-hydrogen two-phase flow in the channel. This induces high heat transfer in the anode channel. As a result, the temperature in the anode falls when the cooling module is turned on while the air outlet temperature remains steady.

The fuel outlet temperature is compared with the stack wall temperatures in Fig. 6. The latter were measured at four different positions of the top, right, left and bottom wall of the stack. Stack wall temperatures increase rapidly from 24.5 to $38\,°C$ during the first 5 min, and then level off until $46\,°C$ is reached, except for the top side wall temperature which rises to $50\,°C$, as high temperature fuel is discharged from the bottom to the top. This trend matches that of the fuel outlet temperature in Fig. 5, but there is a discrepancy throughout the process. It can be estimated that the wall temperature shows real-time follow-up of the MEA temperature due to the high thermal conductivity of carbon graphite and the high heat transfer rate of the fuel from two-phase flow. When the cooling module is turned on, only the top side wall temperature shows a similar trend with the
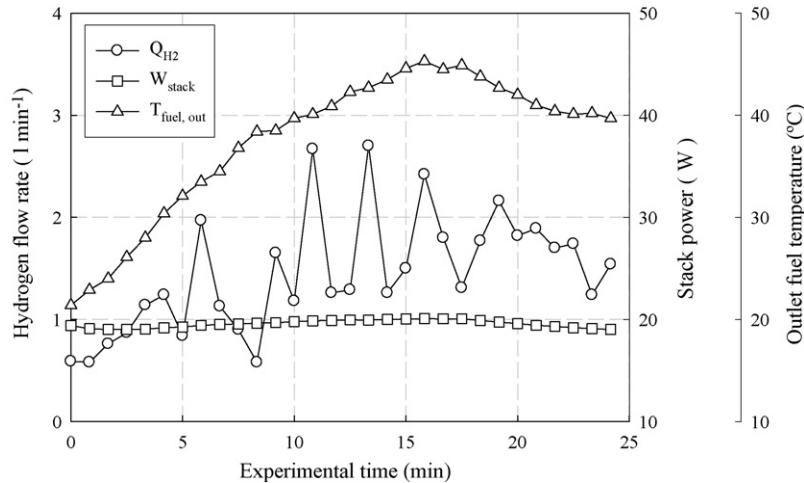
Fig. 8. Hydrogen flow rate, stack power and fuel outlet temperature as function of experimental time. $Q_{air} = 20\,l\,min^{-1}$, $T_{air,in} = 21\,°C$, $H_{air,in} = 100\%$, $Q_{fuel} = 53 \times 10^{-3}\,l\,min^{-1}$, $T_{fuel,in} = 30\,°C$, and $I = 5\,A$.

fuel outlet temperature while the others are not very sensitive. This is because the thermocouple at the top is located close to the cooling module. Thus it reflects the real temperature change when the cooling started while the others show a delay trend from the delayed cooling. According to the sensitive response before and after starting the cooling module, it can be concluded that measuring of the stack wall temperature near the fuel outlet is appropriate for estimation of the real stack condition.

The variation of pressure and pressure loss of the fuel and the air is given in Fig. 7. The air-side pressure increases slowly from 116.4 kPa for about 10 min and peaks at 118.5 kPa, while its pressure loss increases from 14.5 to 16.3 kPa. The increase of pressure loss according to the experimental time results from condensation of high temperature humid air on the relatively low temperature channel. Because saturated air is supplied for cathode oxidant, it causes condensation of water droplets in the cathode channel. The other reason could be a crossover of liquid fuel from the anode [9,10]. At the start of the experiment, the channel is clean and dry. Water droplets form in the channel because of condensation and fuel crossover, and these droplets-coalesce to block the air passage and increase the pressure loss.

The fuel-side pressure and pressure loss exhibit large fluctuations because of active hydrogen generation. The average fuel pressure is 113.2 kPa and its pressure drop is 3.3 kPa. Because of the high fluctuation, it is expected that the fuel-side pressure change will affect the air side, but in fact the effect is negligible. This is because the absolute air pressure is higher than the fuel-side pressure, and the minimum membrane area which is exposed to the fuel and the air channel is sufficiently small to create an effect from the pressure fluctuations. The pressure drop of the air side is 4.9 times higher than that of the fuel side, because the air-side channel is narrower and longer than the fuel channel even though the media density of air is low. Moreover, the net flow rate of the air side is 400 times higher than that of the fuel side.

Fig. 8 shows the trends of the hydrogen flow rate, fuel outlet temperature and stack power. The hydrogen generation rate experiences a large fluctuation because of the imbalance between hydrogen evacuation and generation. The average flow rate reaches $1.9\,l\,min^{-1}$, and then decreases to $1.3\,l\,min^{-1}$ until it levels off. Stack power decreases slightly from 19.4 to 19.0 W during the first 3 min, then it follows a linear increase until it reaches 20.1 W. The slight change of electric power is caused by the characteristics of the electric load. It is set in constant-current mode and the electric load consumes 5 A regardless of the voltage change caused by small variations in the experimental conditions. The same reason causes a rapid voltage decrease after the cooling module is turned on.

The hydrogen generation rate follows the trend of the stack power. According to the increase in stack power, the hydrogen generation rate increases, which causes a rise in fuel temperature. It appears that the increase in fuel temperature accelerates hydrogen generation. The fuel temperature, hydrogen generation rate and stack power are inter-related, and an increase in one factor causes an increase in the others. This is clear from the decrease in hydrogen generation rate, fuel temperature and the output power when the cooling module is started. The trends of the hydrogen generation rate and stack power follow that of the fuel outlet temperature.

The cell voltage and stack power as a function of experimental time are presented in Fig. 9. Each cell voltage decreases slightly for about 3 min from the start. This is due to a maldistribution of the oxidant and the fuel from the sudden influx during the initial period, but it steadily increases for the following 14 min. The average voltage rises to 0.797 V before the cooling module is turned on. The maximum voltage difference among the cells is 0.09 V. Thus it can be concluded that the distribution design of the anode channel is useful for real applications.

3.3. Parametric analysis of five-cell fuel cell stack according to experimental conditions

According to the results of the analysis, key parameters that affect the performance of the five-cell fuel cell stack are hydrogen generation rate, stack wall temperature, fuel outlet temperature and air outlet temperature. To specify the effect
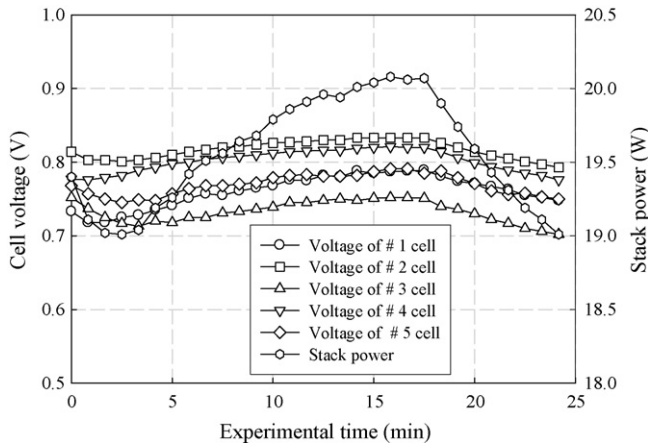
Fig. 9. Cell voltages and stack power as function of time at fixed electric current of 5 A. $Q_{air} = 20 \, l \, min^{-1}$, $T_{air,in} = 21 \, °C$, $H_{air,in} = 100\%$, $Q_{fuel} = 53 \times 10^{-3} \, l \, min^{-1}$, and $T_{fuel,in} = 30 \, °C$.

of parameters over a wider range, the experimental conditions were extended, and the characteristics were analyzed for reproducibility; the results are given in Figs. 10 and 11. The heat pipe-cooling module is turned on when the wall temperature exceeds 70 °C to ensure the safety of the membrane. As shown in Fig. 10, the hydrogen generation rate increases with increase in power density, and can be expressed by

$$Po = 170 \, Q_h^{0.643} \qquad r^2 = 0.740 \tag{2}$$

where Po and Q_h represent the power density and hydrogen generation rate, respectively. The power factor is 0.643, which indicates ineffective power conversion in the region of high hydrogen generation. Active hydrogen generation is expected to promote turbulent flow in the fuel and there by a higher probability for the contact between the fuel and the anode, but the hydrogen generation from the hydrolysis reaction and borohydride electrooxidation reaction are more dominant in the high hydrogen generation region.
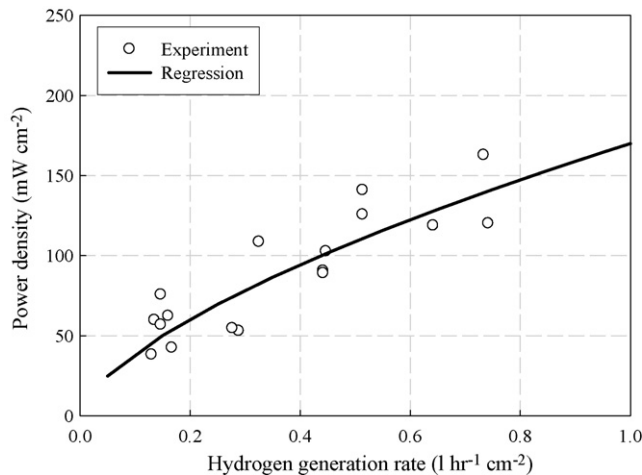

Fig. 10. Power density as function of hydrogen generation rate. $Q_{air} = 10–40 \, l \, min^{-1}$, $T_{air,in} = 19.6–52.2 \, °C$, $H_{air,in} = 100\%$, $Q_{fuel} = 25–101 \times 10^{-3} \, l \, min^{-1}$, and $T_{fuel,in} = 26.3–34.8 \, °C$.
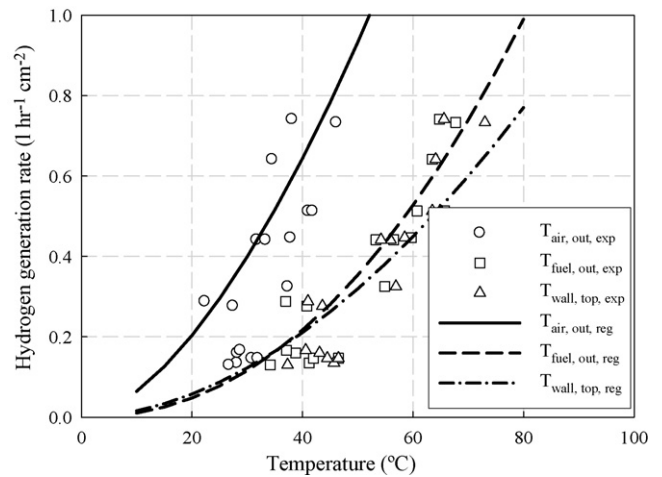

Fig. 11. Hydrogen generation rate as function of temperatures of air outlet, fuel outlet and wall. $Q_{air} = 10–40 \, l \, min^{-1}$, $T_{air,in} = 19.6–52.2 \, °C$, $H_{air,in} = 100\%$, $Q_{fuel} = 25–101 \times 10^{-3} \, l \, min^{-1}$, and $T_{fuel,in} = 26.3–34.8 \, °C$.

Generated hydrogen gas fills part of the volume of the fuel channel and reduces the effective area for the ion passage [7,13]. Hence, an increase in the amount of hydrogen generation will cause cell efficiency to drop rapidly. Fig. 11 displays the hydrogen generation rate as a function of different temperatures of air, fuel and wall. Hydrogen generation is well correlated with the outlet temperatures of air and fuel and the stack wall temperature. According to the heat generation from fuel side, the environmental temperature surrounding the fuel increases, and it accelerates hydrogen generation independent of the increase in stack power. Correlations between the hydrogen generation rate and the temperatures of air, fuel and wall are represented in Eqs. (3)–(5). From these and Eq. (2), it is possible to estimate the stack performance by measuring one of the temperatures:

$$Q_h = 0.0014 \, T_{air,out}^{1.662} \qquad r^2 = 0.596 \tag{3}$$

$$Q_h = 0.000067 \, T_{fuel,out}^{2.191} \qquad r^2 = 0.802 \tag{4}$$

$$Q_h = 0.00021 \, T_{wall}^{1.873} \qquad r^2 = 0.756 \tag{5}$$

where $T_{air,out}$, $T_{fuel,out}$ and T_{wall} represent the temperature of air outlet, fuel outlet and wall, respectively.

Power density is given in Fig. 12 as a function of the temperature of the air outlet, fuel outlet and stack wall. Power density is measured according to the increase and the decrease of temperature by turning on and off the cooling module. The air outlet temperature shows hysteresis according to the decrease of temperature from turning on the cooling module; there is a 10% difference in the maximum power density at the same temperature. On the other hand, the fuel outlet temperature and stack wall temperature represent the stack power well with less hysteresis. A hysteresis of 3% is found in the stack wall temperature, but its absolute value and the variation of power density as a function of stack wall temperatures are well matched with those of the fuel outlet temperature. Thus the stack wall temperature can be used as an index to estimate stack performance. The benefit of using the stack wall temperature as an index of the stack performance is its convenience of measurement in practical usage.
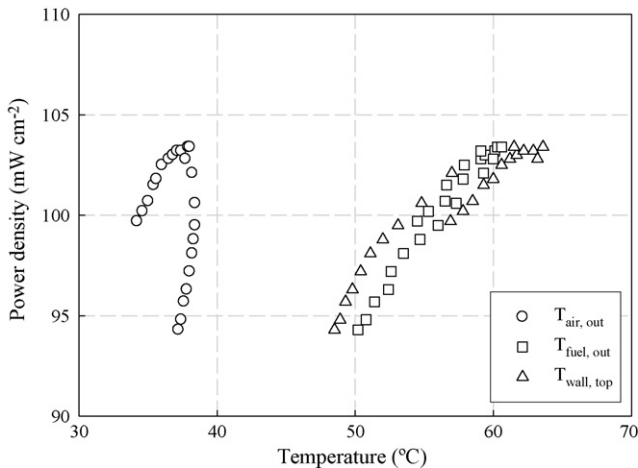
Fig. 12. Power density as function of temperatures of air outlet, fuel outlet and wall at fixed electric current of 10 A. $Q_{air} = 10\,l\,min^{-1}$, $T_{air,in} = 45\,°C$, $H_{air,in} = 100\%$, $Q_{fuel} = 53 \times 10^{-3}\,l\,min^{-1}$, and $T_{fuel,in} = 30\,°C$.
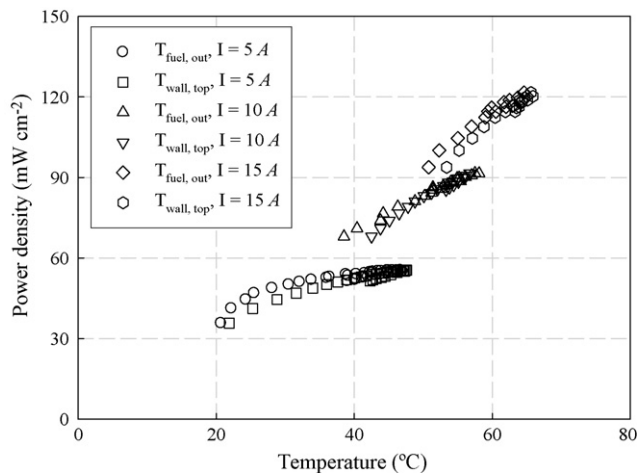

Fig. 13. Power density as function of fuel outlet and wall for different electric currents. $Q_{air} = 10\,l\,min^{-1}$, $T_{air,in} = 20\,°C$, $H_{air,in} = 100\%$, $Q_{fuel} = 53 \times 10^{-3}\,l\,min^{-1}$, and $T_{fuel,in} = 28\,°C$.

The power density is shown in Fig. 13 as a function of the temperature of fuel and wall for different electric currents. It is clear that the fuel outlet temperature and the stack wall temperature are main indices to estimate stack performance. The gradient becomes steeper with increase in current, because the stack efficiency decreases concomitantly. Thus the change in temperatures is more severe in a high current region.

4. Conclusions

Carbon graphite can be used for the purpose of DBFC weight reduction, even though there is a 12% performance degradation in a single cell as a consequence of inadequate material strength. This is caused by insufficient contact between the end-plate and MEA from a lack of stacking force. As a result, stack weight can be decreased by a factor of 4.2 compared with that of stainless steel.

The performance of the stacked cell exceeds that of a single cell because of the increase in temperature of the former due to the reduction of radiation area from the narrow stacking of cells. Key parameters indicating the stack performance are stack wall temperature, fuel outlet temperature, air outlet temperature and hydrogen generation rate. In particular, the top side stack wall temperature can be used as an index of the stack performance in the view of its convenience of measurement.

An internal manifold and a parallel-type anode channel are effective for the stacking of a DBFC, because the deviation from the maximum cell voltage in the stack is within 0.09 V. It appears the reduction of the fuel-side pressure loss enhances the performance of the five-cell fuel cell stack.

References

[1] J.Y. Lee, H.H. Lee, J.H. Lee, D.M. Kim, US Patent 5,599,640 (1997).
[2] S. Amendola, US Patent 5,8043,29 (1998).
[3] S. Amendola, C.P. Onnerud, M.T. Kelly, P.J. Petillo, S.L. Sharp-Goldman, M. Binder, J. Power Sources 84 (1999) 130.
[4] S.C. Amendola, S.L. Sharp-Goldman, M.S. Janjua, N.C. Spencer, M.T. Kelly, P.J. Pdtillo, M. Binder, Int. J. Hydrogen Energy 25 (2000) 969.
[5] S. Suda, US Patent 6,358,488 B1 (2002).
[6] Z.P. Li, B.H. Liu, J.K. Zhu, S. Suda, J. Power Sources 163 (2006) 555.
[7] K.T. Park, U.H. Jung, S.U. Jeong, S.H. Kim, J. Power Sources 162 (2006) 192.
[8] J.H. Wee, J. Power Sources 161 (2006) 1.
[9] J.H. Wee, J. Power Sources 155 (2006) 329.
[10] C. Ponce de Leon, F.C. Walsh, D. Pletcher, D.J. Browning, J.B. Lakeman, J. Power Sources 155 (2006) 172.
[11] M. Chatenet, F. Micoud, I. Roche, E. Chainet, J. Vondrak, Electrochim. Acta 51 (2006) 5452.
[12] M.H. Atwan, C.L.B. Macdonald, D.O. Northwood, E.L. Gyenge, J. Power Sources 158 (2006) 36.
[13] H. Cheng, K. Scott, J. Power Sources 160 (2006) 407.
[14] Y. Kojima, K. Suzuki, K. Fukumoto, M. Sasaki, T. Yamamoto, Y. Kawai, H. Hayashi, Int. J. Hydrogen Energy 27 (2002) 1029.
[15] Y. Kojima, Y. Kawai, M. Kimbara, H. Nakanishi, S. Mstsumoto, Int. J. Hydrogen Energy 29 (2004) 1213.
[16] B.H. Liu, Z.P. Li, S. Suda, J. Alloys Compd. 415 (1–2) (2006) 288.
[17] M.Y. Ha, C.H. Kim, Y.W. Jung, S.G. Heo, J. Mech. Sci. Technol. 20 (6) (2006) 840.
[18] Z.P. Li, B.H. Liu, K. Arai, S. Suda, J. Alloys Compd. 404–406 (2005) 648.
[19] C.H. Kim, K.J. Kim, S.C. Ha, T.H. Cho, M.S. Park, M.H. Lee, S.T. Ko, S.G. Heo, Korea Patent 10-0,486,598 (2005).
[20] C.H. Kim, Ph.D. Thesis, Pusan National University, 2007, p. 117.
[21] J.H. Koh, H.K. Seo, C.G. Lee, Y.S. Yoo, H.C. Lim, J. Power Sources 115 (2003) 54.
[22] K.P. Robert, W. Brian, US Patent 6,887,606 B2 (2005).